



In Situ Synthesis and Characterization of Conductive Hybrid Composites Using Functionalized 3D Molybdenum Disulfide Nanoflowers

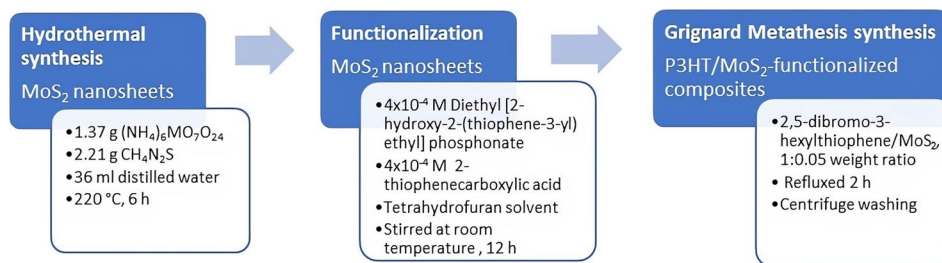
S. García-Carvajal¹ · M. E. Nicho² · D. Hernández-Martínez³ · M. Fuentes-Pérez² · J. Nicasio-Collazo⁴ · V. Ruiz-Santoyo¹ · M. C. Arenas-Arrocena¹

Received: 12 January 2024 / Accepted: 27 March 2024
© The Author(s) 2024

Abstract

We obtained 3D nanoflowers of MoS₂ (3D-MoS₂) with an average size of 1–3 μm synthesized by a one-step hydrothermal method, the "flower-shape" being composed of several petal-like sheets with a thickness of about 19 nm. The 3D nanoflowers underwent functionalization with diethyl[2-hydroxy-2-(thiophen-3-yl)ethyl]phosphonate and 2-thiophene carboxylic acid. P3HT/MoS₂ composites were synthesized by Grignard metathesis using a 2,5-dibromo-3-hexylthiophene/MoS₂ weight ratio of 1:0.05. As a reference, the P3HT/MoS₂ composites were also synthesized with unfunctionalized 3D-MoS₂. The P3HT/MoS₂ composites were characterized by FTIR, XRD, TEM, ¹H NMR, UV–Vis, TGA, and cyclic voltammetry. We studied the influence of 3D-MoS₂ nanoflowers functionalized with phosphonic and carboxyl groups on the properties of the P3HT/MoS₂ composites. The addition of functionalized 3D-MoS₂ in the P3HT/MoS₂ composites improved the percentage of HT dyads and the definition of shoulders in the dyad signal, indicating a better arrangement of the polymeric chains in the P3HT/3D-MoS₂ functionalized composites. In addition, the functionalization of the 3D-MoS₂ with phosphonic group increased the conjugation length, the percentage of crystallinity, and the conductivity. Likewise, the P3HT/MoS₂ functionalized composites showed a decrease in the energy gap compared to P3HT. The functionalization of the 3D-MoS₂ was successfully carried out, and a close interaction between the P3HT and 3D-MoS₂ was determined. We achieved the in situ synthesis of P3HT/MoS₂ composites by Grignard metathesis using functionalized 3D-MoS₂ obtained by the hydrothermal method. We compared two functionalization groups with 3D-MoS₂ and their subsequent polymerization with P3HT. Our work provides evidence for a better performance in composites functionalized with a phosphonate group because a phosphonic anchor provides strong electronic coupling with the 3D-MoS₂. The above makes this material suitable for applications in flexible electronics photosensors, electrochromic devices, photocatalysis, and harvesting energy material in solar cells.

Graphical Abstract



Keywords Composite · functionalization · molybdenum disulfide · poly(3-hexylthiophene) · semiconductive polymer

Extended author information available on the last page of the article

Introduction

Molybdenum disulfide (MoS_2) nanostructures are widely acknowledged as prominent representatives within the category of transition metal dichalcogenides (TMDs). These nanostructures display a diverse array of properties as they transition from the macroscopic to the nanoscale, rendering them highly promising materials with multifunctional properties.^{1,2}

MoS_2 , an *n*-type semiconductor in bulk form is a TMD with an energy band gap of 1.3 eV which changes to 1.8 eV in monolayer form. Similarly, when MoS_2 cleaved from bulk to monolayer, the energy band transforms from an indirect to a direct transition due to the quantum confinement effect. The room-temperature carrier mobility of the MoS_2 monolayer is $200 \text{ cm}^2 \text{V}^{-1} \text{ s}^{-1}$ with a high on/off current ratio of $\sim 10^8$.^{3,4} Given these attributes, MoS_2 exhibits considerable promise for diverse applications, including lubricants and grease additives, lithium-ion batteries, catalysts in water-splitting, biosensors, bioimaging, transistors, memory devices, flexible electronics photodetectors, energy storage and conversion, and the hydrogen evolution reaction.^{4,5,6}

There are several methods to synthesize layered TMDs,⁷ and different MoS_2 nanostructures, including nanospheres, nanosheets, nanotubes, nanorods, and flower-like structures, have been synthesized using a variety of techniques, such as spray pyrolysis, thermal evaporation, chemical vapor deposition, electrochemical deposition, chemical reduction, radio frequency sputtering, precipitation, and hydrothermal.^{3,7,8} Most techniques used to synthesize nanostructures are complex and highly expensive. However, the hydrothermal method offers a simple, environmentally friendly, and cost-effective approach to synthesize inorganic nanomaterials at low temperatures, obtaining high yield, good crystallinity, and tunable morphology⁸. also offering more control over the size, shape, and composition of the nanostructures and not requiring expensive equipment or facilities.⁹ For energy storage devices, 3D nanostructures are always attractive compared to 2D nanostructures because they have less aggregation and agglomeration and thus can sustain the superior intrinsic characteristics of nanomaterials, such as high surface area, unique physical properties, and structural stability.¹⁰ The hydrothermal method has the potential for mass production and is therefore extensively employed for the large-scale production of 3D MoS_2 nanostructures,^{9,11} and has also been employed for the preparation of novel 3D nanoflowers formed with few-layered and expanded interlayer spacing MoS_2 .¹² The ability to modulate the band gap by adjusting the thickness of the MoS_2 layer makes few-layer MoS_2 films highly advantageous

as photovoltaic materials for the efficient absorption of solar energy.¹³ The advantages, such as shorter diffusion pathways, heightened electronic properties, and larger active surface areas, in 3D- MoS_2 represents the key for the improvement of the photodegradation activity performance and gas sensitivity. and may provide a new perspective in view of the applicability for different environmental applications.^{14,15} To enhance the electrical, thermal, mechanical, and flame-retardant properties, several polymers have been combined with MoS_2 nanosheets.^{16–21} There are many reports on MoS_2 and polymers for sensing and solar cell applications: PMMA- MoS_2 and PANI- MoS_2 - SnO_2 as an ammonia gas sensor;^{22,23} PVP- MoS_2 -ZnO composite for hydrogen gas sensing;²⁴ MoS_2 applied in composites with PANI/ MoS_2 ^{25,26} and polythiophene/ MoS_2 ²⁷ as a counter electrode in dye-sensitized solar cell-based counter electrodes.

P3HT, a polymer semiconductor, has gained significant popularity as a donor material in organic electronic devices. This is primarily attributed to its favorable attributes, such as chemical and electrochemical stability, suitable energy level, high electrical conductivity, and solubility in various solvents.^{28,29} P3HT/ MoS_2 composites have been synthesized by physical mixing for ammonium sensing,^{30,31} Xie et al.³¹ studied different sensitive film structures as active layers in an organic thin-film transistor ammonia (NH_3) sensor, i.e., P3HT- MoS_2 composite film, P3HT/ MoS_2 bilayer film, and MoS_2 /P3HT bilayer film were fabricated by spray technology, and gas sensors based on P3HT- MoS_2 composite film showed a shorter recovery time than other sensors, which was attributed to the closer interlayer d-spacing and π - π stacking of the P3HT chains in the composite film due to the MoS_2 being doped.³¹ Kandpal et al. investigated interlayer-applied MoS_2 as a dopant in P3HT for electrochromic devices.^{32,33} Prakash et al. reported significantly improved mobility of the P3HT when added to MoS_2 as a dopant in organic field-effect transistors.³⁴

MoS_2 nanoparticles in an organic semiconductor (MoS_2 /P3HT) composite applied in a hybrid dye for thin-film transistors enhanced the film crystallinity.³⁵ P3HT loaded with 1 wt% MoS_2 showed an enhancement in the self-assembly of polymers in the form of a fibrillar formation and excellent structural features in terms of π -conjugation to a self-powered photodetector.³⁶ MoS_2 /P3HT composites have shown an enhancement of capacitance and excellent cycle stability when used in a supercapacitor.³⁷ In solar cells, a P3HT/ MoS_2 interface layer provides much better device stability than that of P3HT, and results in drastic (41%) efficiency enhancement through efficient charge extraction.³⁸

Reports of P3HT/ MoS_2 composites are very extensive, the majority involving 2D MoS_2 nanoparticles by chemical exfoliation, with the experimental method of the composites carried out by physical mixing, so that

they all agree by showing increases in their crystallinity properties, charge mobility, and better arrangement of interlayer d-spacing and π - π stacking of the P3HT chains due to the MoS₂. P3HT/3D-MoS₂ composites are less commonly reported, with 3D-MoS₂ being used as an interlayer-improved electrochromic performance of the device with P3HT,^{32,33,39} whereas, in FTO/TiO₂/MoS₂-P3HT/PEDOT:PSS/Ag solar cells, it increased the energy conversion efficiency (1.28%) by only about 58% in comparison to solar cells based on TiO₂/P3HT.⁴⁰ Thus, further research on the in situ synthesis of P3HT/MoS₂ composites with 3D-MoS₂ is required.

Considering the studies previously reported and with the aim of achieving an optimal performance in polymer/MoS₂ nanocomposites, it is crucial to ensure the uniform dispersion of the MoS₂ nanosheets within the polymer matrix, and to establish appropriate interfacial interactions between the nanosheets and the surrounding matrix.⁴¹ To improve the dispersion, organic ligands are required which can bind to the MoS₂ surface through a covalent bond, which opens a promising way for the development of covalently functionalized MoS₂/polymer nanocomposites.⁴² Several techniques have been developed to enhance the dispersion of MoS₂, which can be employed to incorporate the MoS₂ into polymers, such as covalent functionalization, non-covalent, in situ polymerization, and physical blending. These methods aim to improve the distribution of MoS₂ particles within the polymer matrices.⁴³ On the other hand, covalent bonds can be formed between the MoS₂ surface and a range of organic groups, offering an exciting opportunity for the advancement of covalently functionalized MoS₂/polymer nanocomposites. This avenue holds great potential for the development of these hybrid materials.⁴³

As far as our understanding goes, there is no currently available literature discussing the in situ synthesis of conductive polymers of 3D nanoflowers made of functionalized MoS₂. Our research team has successfully dispersed functionalized inorganic CdS nanoparticles directly into a 3HT monomer solution, which was achieved by employing a functionalizing anchor (diethyl[2-hydroxy-2-(thiophene-3-yl)ethyl]phosphonate), prior to the polymerization synthesis. The purpose of this approach was to prevent phase segregation of the nanoparticles and their rapid sedimentation within the polymer.^{44,45} A few studies have been reported on the functionalization of P3HT using organic ligands, such as phosphonic ester,⁴⁶ pyridines, thiols,^{47,48} and phenols.^{47,49} The surface of TiO₂ nanoparticles was modified by utilizing 2-thiophene carboxylic acid to create self-assembled monolayers. This step facilitated the subsequent surface oxidative graft polymerization, resulting in the formation of compact P3HT layers.⁵⁰

In this work, we present a methodology for synthesizing 3D-MoS₂ nanoflowers through the hydrothermal method.

Additionally, the functionalization of 3D-MoS₂ nanoflowers with two organic groups, diethyl[2-hydroxy-2-(thiophene-3-yl)ethyl] phosphonate, and 2-thiophene carboxylic acid, as well as the nanocomposites, are proposed by in situ synthesis of P3HT with 3D-MoS₂ nanoflowers (functionalized and non-functionalized). The functionalization of 3D-MoS₂ nanoflowers offers better interfacial interactions between the 3D nanoflowers and the polymeric matrix of P3HT, such as shorter diffusion pathways and, heightened electronic properties of P3HT/3D-MoS₂ functionalized composites.

Experimental

Hydrothermal Synthesis of (3D-MoS₂) Nanoflowers

3D-MoS₂ was synthesized by a one-step hydrothermal method according to Zhang et al.⁵¹ Amounts of 1.37 g of hexaammonium heptamolybdate tetrahydrate ((NH₄)₆Mo₇O₂₄) purchased from Sigma-Aldrich and 2.21 g of thiourea SC(NH₂)₂ purchased from Fermont were used. The substances were dissolved in 36 ml of distilled water while vigorously stirring for a duration of 30 min, resulting in the formation of a uniform solution, which was then transferred to a 150-ml Teflon-lined stainless-steel autoclave, tightly sealed, and subjected to heating at 220°C for 6 h. After the heating process, the solution was cooled to room temperature. The resulting black precipitates were collected through centrifugation and underwent multiple washes with ethanol and distilled water. Subsequently, they were dried at room temperature for 72 h and finally ground in an agate mortar to obtain the desired product.

P3HT/3D-MoS₂ Functionalized Composites

Synthesis of Diethyl [2-Hydroxy-2-(Thiophene-3-yl)Ethyl] Phosphonate.

The functionalizing agent, diethyl [2-hydroxy-2-(thiophene-3-yl)ethyl] phosphonate, was synthesized using a procedure similar to the one previously reported by Linzaga-Elizalde et al.^{45,52} The 2-thiophenecarboxylic acid as a functionalizing agent was purchased from Sigma-Aldrich (99% purity).

Functionalization of 3D-MoS₂ Nanoflowers

3D-MoS₂ were added to a 4 × 10⁻⁴ M solution of each functionalizing agent (diethyl [2-hydroxy-2-(thiophene-3-yl)ethyl] phosphonate or 2-thiophene carboxylic acid), in tetrahydrofuran, and the mixture was stirred for 12 h at room temperature. The functionalized 3D-MoS₂ was then filtered

and washed with tetrahydrofuran to remove any bonded agents.^{45,50}

Synthesis of P3HT/MoS₂ Functionalized Composites

Grignard metathesis synthesis of P3HT/MoS₂ composites was carried out by using a 2,5-dibromo-3-hexylthiophene/3D-MoS₂ at the weight ratio of 1:0.05. 2,5-dibromo-3-hexylthiophene (1.5 ml, 6.996 mmol) and anhydrous tetrahydrofuran (THF) (11 ml) were combined in a dried 250-ml three-neck round-bottom flask under N₂ gas with functionalized 3D-MoS₂ nanoflowers (0.12 g, 0.750 mmol). Prior to this, the 3D-MoS₂ nanoflowers were dispersed in anhydrous THF using an ultrasonic bath and then introduced into the reaction mixture, which was stirred for 5 min and refluxed under a nitrogen atmosphere for 1 h. Dodecylmagnesium bromide (1.0 M solution in diethyl ether, 5.6 mmol) was subsequently added using a deoxygenated syringe, and the resulting mixture was gently refluxed for 1 h. Following refluxing and stirring under nitrogen, [1,3-bis(diphenylphosphino)propane] dichloronickel(II) [(1,3-dppp)NiCl₂] (0.03 g, 0.055 mmol) was introduced. Next, the mixture was subjected to reflux for a duration of 2 h. To isolate the composite, 250 ml of methanol was added to the solution, followed by filtration. The resulting polymer was then washed with methanol and hexane through centrifugation, and subsequently dried for 48 h at 55°C. The synthesis of the P3HT/MoS₂ composites using Grignard metathesis followed a procedure previously studied by Hernández-Guzmán et al.⁵³

The composite obtained by synthesis of 3D-MoS₂ functionalized with diethyl[2-hydroxy-2-(thiophene-3-yl)ethyl]phosphonate has been named P3HT/MoS₂-EF, the composite produced with 3D-MoS₂ functionalized using 2-thiophene carboxylic acid has been named P3HT/MoS₂-CF, and the composite synthesized without functionalization of 3D-MoS₂ has been named P3HT/MoS₂. A pristine P3HT sample was also prepared following the same procedure but without the addition of 3D-MoS₂. Films of the composites and the polymer were deposited by spin-coating on Corning glass substrates at a rotation speed of 2000 rpm from chlorobenzene solutions with a concentration of 4 mg/ml. The chemical structures of the P3HT and the P3HT/MoS₂ composites are shown in Fig. 1.

Characterization

The morphologies of the synthesized products were examined using transmission electron microscopy (TEM; JEM-1010; JEOL). The determination of dyad and triad contents in the P3HT polymer and P3HT/MoS₂ composites was performed using hydrogen nuclear magnetic resonance (¹H NMR; Mercury 200 MHz; Varian). Deuterated chloroform

(CDCl₃) was used as the solvent, and trimethyl silane served as an internal reference. Fourier-transform infrared (FTIR; Frontier FTIR; Perkin Elmer) spectra with attenuated total reflection (ATR) were conducted in the range of 4000–400 cm⁻¹. UV-Vis spectra (Multiskan GO; Thermo Scientific) covered the wavelength range of 200–1100 nm. X-ray diffraction (XRD; D2 Phaser; Bruker) analysis was carried out with Cu Kα (λ = 1.5418 Å) radiation, operating at 10 kV and 5 mA. The samples were subjected to an angular sweep from 10° to 60° with a standard increment of 0.02°. Thermogravimetric analysis (TGA; TA Q500) was employed to determine the thermal stability and decomposition temperature under a nitrogen atmosphere. The samples were heated at a rate of 10°C/min.

Cyclic voltammetry (electrochemical characterization) was recorded with a BAS epsilon 100 B/W potentiostat/galvanostat, and a scanning rate of 20 mV/s was used. A three-electrode system was used. The working electrode was an ITO substrate coated with P3HT or the P3HT/MoS₂/ITO composite films, the counter electrode was a platinum mesh, and Ag/Ag⁺ (0.1 M Ag/AgNO₃) was used as the reference electrode. The electrochemical bath consisted of a non-aqueous medium (0.1 M LiClO₄ in ACN) for a potential range of –200 to 1200 mV.

Results and Discussion

TEM Analysis

Figure 2 depicts the TEM images of 3D-MoS₂, P3HT, and P3HT/MoS₂ composites. Figure 2a, b reveals a morphology of nanoflowers with dimensions ranging from 100 to 300 nm. The structure of each "flower" consists of numerous petal-like lamellae, approximately 19 nm thick. The software ImageJ was utilized to calculate the size distributions (diameters) of both the flower-like nanostructures and each individual petal-like lamella. The nanoflower distribution size and thickness of the lamellae correspond to reports of 3D flower-like spheres.^{32,49,51} On the other hand, P3HT shows the typical morphology for this class of polymer (Fig. 2c, d). When 3D-MoS₂ nanoflowers are added to the P3HT polymer matrix, all the composites showed the integration of MoS₂ into the P3HT morphology. When MoS₂ was added into P3HT, an agglomerate morphology appeared in the polymer, which may be due to the incorporation and interaction between P3HT and 3D-MoS₂ (Fig. 2e–j).

This verifies that the functionalization of the 3D-MoS₂ nanoflowers was carried out successfully and also verifies a close interaction between the P3HT and 3D-MoS₂ nanoflowers. Sun et al. reported on a TEM analysis of P3HT/MoS₂ by physical mixture,⁴⁰ the results indicating the presence of 3D-MoS₂ in P3HT, which did not present changes

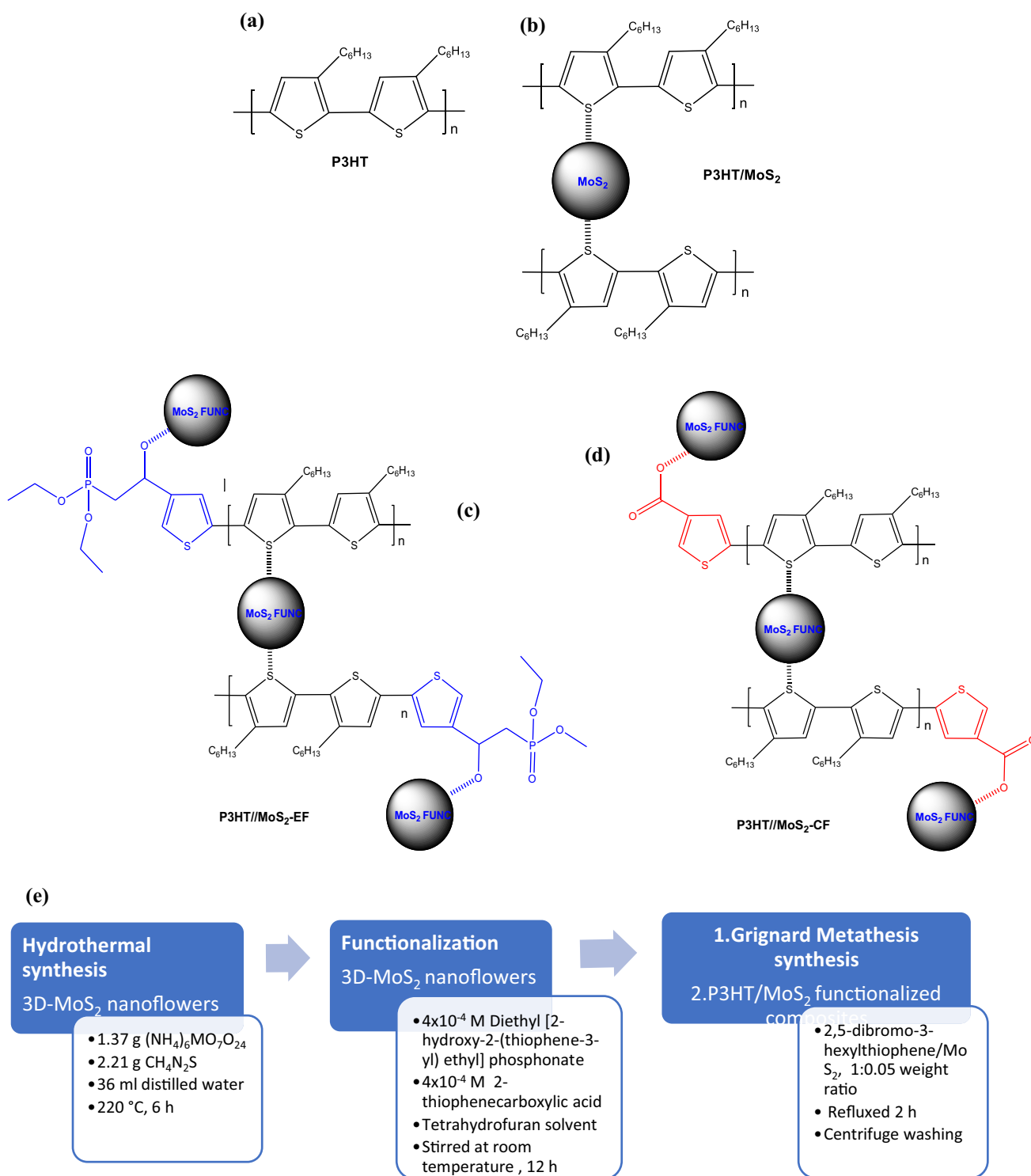


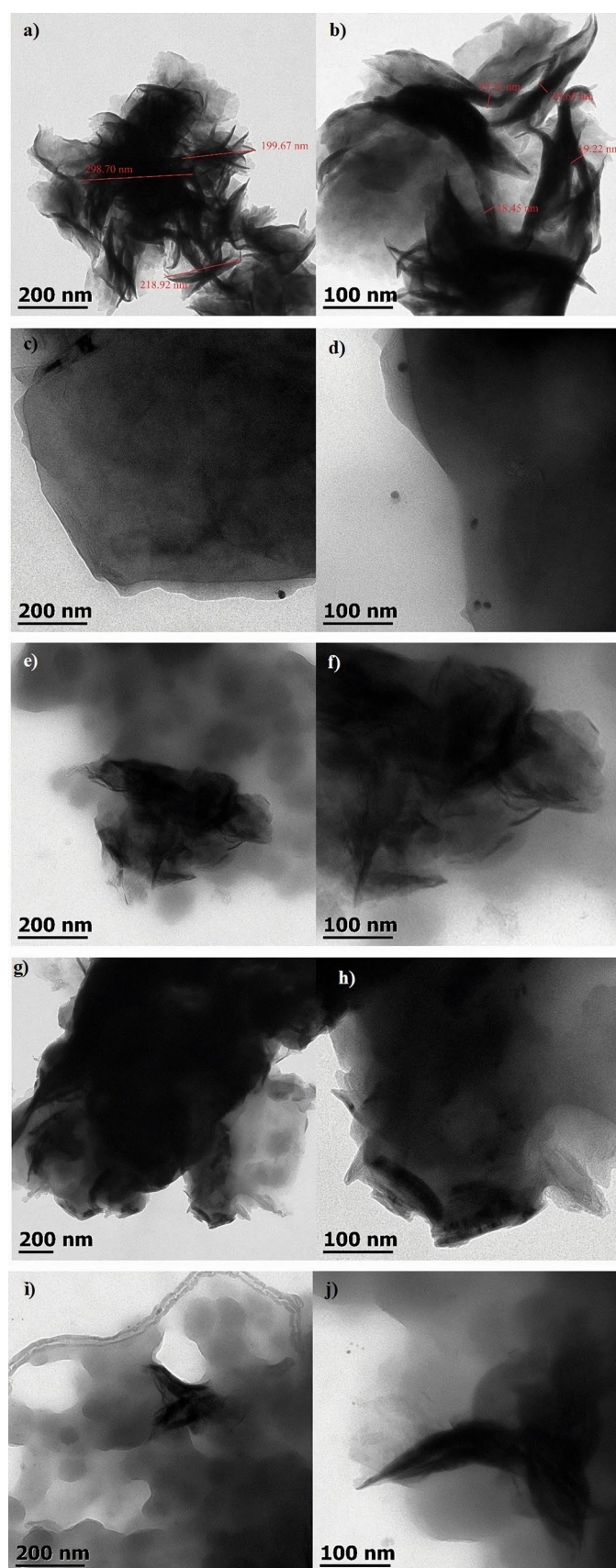
Fig. 1 Chemical structures of (a) P3HT, (b) P3HT/MoS₂ with 3D-MoS₂ non-functionalized, (c) P3HT/MoS₂ with 3D-MoS₂ functionalized with diethyl [2-hydroxy-2-(thiophene-3-yl)ethyl] phospho-

nate, P3HT/MoS₂-EF, (d) P3HT/MoS₂ with 3D-MoS₂ functionalized with 2-thiophene carboxylic acid, P3HT/MoS₂-CF, and (e) methodology for obtaining functionalized composites.

in morphology with added 3D-MoS₂. In our case, P3HT in all the composites presented an agglomerated morphology more defined when they were functionalized, especially

the composite P3HT/MoS₂-EF, perhaps because there is a better interaction between the polymer chains of P3HT and 3D-MoS₂. The in situ synthesis by the Grignard metathesis

Fig. 2 (a, b) TEM images of 3D-MoS₂ nanoflowers, (c, d) P3HT pristine, (e, f) P3HT/MoS₂ non-functionalized, (g, h) P3HT/MoS₂-EF, and (i, j) P3HT/MoS₂-CF.



method is commonly used to synthesize P3ATs, so the improvements in the material properties obtained based on this method are easily scalable,⁵⁴ and this is the conventional method providing growth sites for P3HT nanowires, increasing the interfacial adhesion between the nanoparticles and the polymer matrix.⁵⁵ Verma et al. confirmed that the morphology in P3HT/MoS₂ nanocomposite was nanofibrous compared to the pristine P3HT (smooth morphology), and that the surface morphology and charge transfer characteristics are due to conjugated π - π electron coupling, improving the polaron delocalization over channel length, thus enhancing the charge transport facility and mobility.³⁰

¹H NMR Analysis

Figure 3 illustrates the ¹H NMR spectra of P3HT and P3HT/MoS₂ composites. In the spectra, signals appearing between 2.50 and 3.0 ppm correspond to the methylene group directly linked to the thiophene ring, indicating a dyad configuration (Fig. 2a). The relative proportions of head-head (HH) and head-tail (HT) dyads in the P3HT polymer and P3HT/MoS₂ composites were estimated by analyzing the area under the

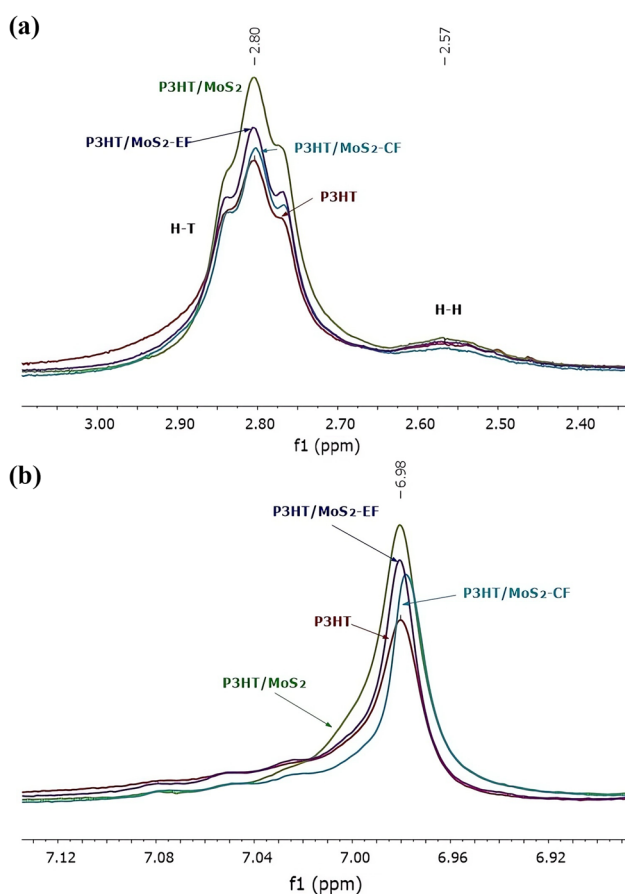


Fig. 3 ¹H NMR analysis of P3HT and P3HT/MoS₂ composites: (a) dyads and (b) triads.

curve of the signals observed around $\delta = 2.57$ ppm (HH) and 2.80 ppm (HT). The results of the displacement are summarized in Table I. The presence of 3D-MoS₂ in P3HT led to a reduction in the HT dyad content in the case of non-functionalized 3D-MoS₂ (P3HT/MoS₂). However, when 3D-MoS₂ was functionalized, the percentage of HT dyads in the P3HT/MoS₂-CF and P3HT/MoS₂-EF composites was like that of pure P3HT, suggesting that the arrangement of P3HT chains is unaffected by the presence of functionalized 3D-MoS₂, which is in accordance with CdS functionalized with diethyl [2-hydroxy-2-(thiophene-3-yl)ethyl] phosphonate in P3HT composites.⁴⁵

The signals observed between $\delta = 6.0$ ppm and $\delta = 7.10$ ppm in the spectra correspond to the methyne α to methylene on the thiophene ring, providing insights into the configuration of the triads (Fig. 3b). The signals corresponding to the dyads (Fig. 3a) and triads (Fig. 3b) in the P3HT/MoS₂ composite exhibited broadening, which was attributed to the direct interactions between P3HT and 3D-MoS₂ nanoflowers within the composite, as well as the aggregation effects of the polymer chains surrounding the nanoflowers. Similar peak broadening has been reported in other P3HT/nanostructured composites.^{56,57} The relationship in the broadening of the signal was low in the functionalized composites because the functionalizing agent interferes between the 3D-MoS₂ nanoflowers and P3HT, corroborating the functionalization of the 3D-MoS₂ nanoflowers. The P3HT/MoS₂-EF presented a larger broadening than P3HT/MoS₂-CF. The phosphonic anchor group is more competitive in binding to the surface of up-conversion nanoparticles than the carboxylic acid group.⁵⁸ Zhang et al. reported that the phosphonic acid anchor provides strong electronic coupling with the TiO₂ semiconductor,⁵⁹ the P3HT/MoS₂-EF probably presented a strong electronic coupling with the 3D-MoS₂ nanoflower, and therefore presented more aggregation effects of the polymer chains surrounding the nanoflowers than P3HT/MoS₂-CF. These results agree with the TEM.

Functionalized composites show a shifting effect on the maxima peak of dyad and triad signals (mostly in triads) at a greater (P3HT/MoS₂-CF) or lesser (P3HT/MoS₂-EF) field (Fig. 3b) compared to P3HT. This may be related to the fact that the methylene of thiophene could be affected by the protection and deprotection effect of the functionalized

Table I Dyad percentages for P3HT/MoS₂ composites and P3HT polymer

| Sample | HT % | HH % |
|---------------------------|-------|-------|
| P3HT | 87.31 | 12.69 |
| P3HT/MoS ₂ | 85.30 | 14.70 |
| P3HT/MoS ₂ -EF | 87.29 | 12.71 |
| P3HT/MoS ₂ -CF | 86.89 | 13.11 |

3D-MoS₂, caused by the presence of the ethyl ester of the phosphonic and carboxyl groups of the functionalizing agent. Additionally, this also corroborates the functionalization of the 3D-MoS₂, as well as the incorporation of 3D-MoS₂ into P3HT. The composite P3HT/MoS₂-CF showed the largest shift (δ) in the triad signal.

According to the literature, the presence and definition of shoulders in the dyad signals of P3HT indicate a better order of the polymer chains.^{54,57,60} All P3HT/MoS₂ composites showed shoulders in the HT dyad signal, and P3HT/MoS₂ composites functionalized present better definition of the shoulders than P3HT/MoS₂ and P3HT, which indicates a better order of polymer chains in the functionalized composites.

FTIR-ATR Analysis

Figure 4 shows the FTIR-ATR spectra of the nanostructures of 3D-MoS₂, P3HT, and P3HT/MoS₂ composites. In the 3D-MoS₂ spectrum, asymmetric stretching vibrations of C-NH-C were observed at 1129 cm⁻¹ and 1414 cm⁻¹, while vibrational absorption bands at 1633 cm⁻¹ and 1100 cm⁻¹ were attributed to Mo-O vibration and the stretching of the O-H bond, respectively.⁶¹ Vibrational bands at 909 cm⁻¹ and 656 cm⁻¹ were assigned to the S-S bond and Mo-S bond, respectively, which are characteristic fingerprints of MoS₂.^{27,61}

On the other hand, the spectrum of the P3HT polymer presented stretching vibrations (symmetric and asymmetric) corresponding to C = C bonds at 1454 and 1510 cm⁻¹. The bending of the methyl groups is represented by a band at 1374 cm⁻¹, the stretching of C-S bonds is represented by

a band at 1112 cm⁻¹, and, in a 2,3,5-trisubstituted ring, the band at 818 cm⁻¹ is associated with the out-of-plane vibration of aromatic C-H bonds, and the vibration of methylene groups -(CH₂)₅- in the hexyl substituent is assigned to the band at 723 cm⁻¹.⁶²⁻⁶⁴

The characteristic bands of P3HT were observed in all composite P3HT/MoS₂ spectra, indicating the presence of the polymer in the composites. The successful polymerization of 2,5-dibromo-3-hexylthiophene in the presence of 3D-MoS₂ nanoflowers was verified by the band observed at 818 cm⁻¹ associated with out-of-plane vibration of the 2,3,5-trisubstituted thiophene ring. Additionally, the presence of 3D-MoS₂ nanoflowers was confirmed in P3HT/MoS₂ composites by bands at 1633 and 1100 cm⁻¹, as they were correlated with the Mo-O vibration and O-H stretching, respectively. The S-S and Mo-S bonds were observed by typical bands at 909 cm⁻¹ and 456 cm⁻¹, further supporting the presence of 3D-MoS₂ nanoflowers in the composites as fingerprint characteristics of MoS₂.⁶¹

A proof of the interaction of the 3D-MoS₂ with P3HT is the increase in the intensity of the band at 1092 cm⁻¹ (Fig. 4b), a fact observed mainly in the P3HT/MoS₂-EF and P3HT/MoS₂-CF functionalized composites. In previous work, it has been reported that the incorporation of CdS nanostructures into P3HT leads to the broadening of the band related to the C-S stretching, resulting in two distinct peaks. Interestingly, with increasing CdS concentration, the intensity of the peak at 1087 cm⁻¹ was also increased.^{44,65} Furthermore, the functionalized CdS nanoparticles induce a more pronounced shift of the peak at 1087 cm⁻¹ towards lower wave numbers, accompanied by a higher intensity.⁴⁵ Relative to P3HT, the P3HT/MoS₂-CF and P3HT/MoS₂-EF

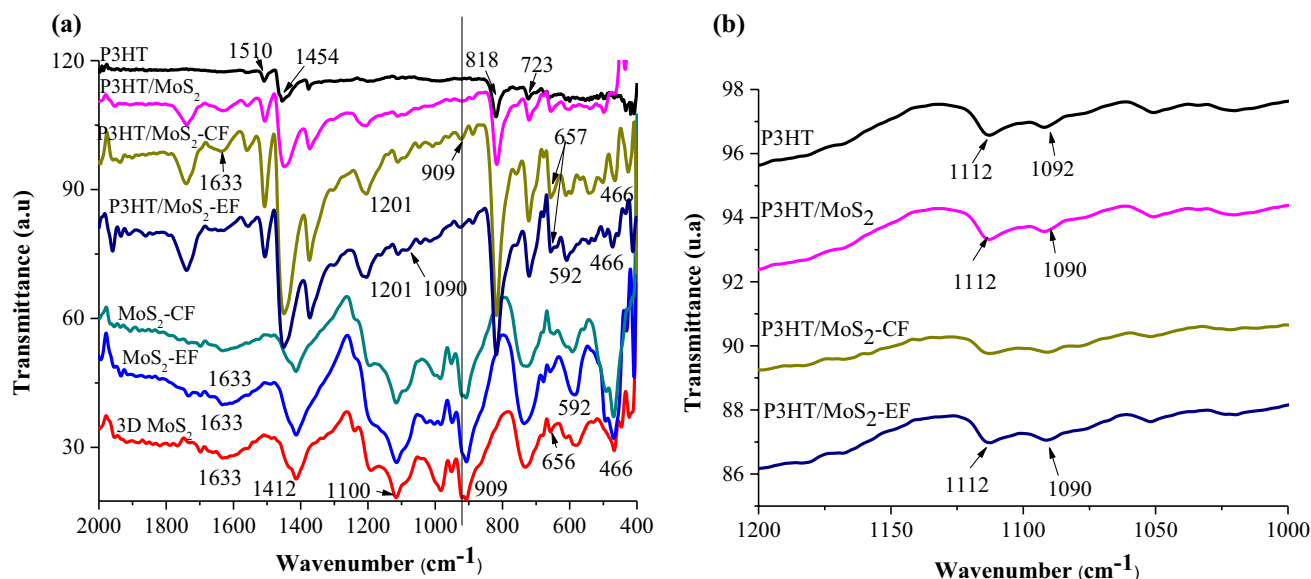


Fig. 4 FTIR-ATR spectra of 3D-MoS₂, P3HT polymer, P3HT/MoS₂ composites: (a) 2000 cm⁻¹ to 400 cm⁻¹ and (b) 1200 cm⁻¹ to 1000 cm⁻¹.

composites also showed a peak shift from 1092 cm^{-1} to 1090 cm^{-1} . It is worth mentioning that, even though all the composites (functionalized and non-functionalized) have the same concentration of 3D-MoS₂, in the case of the functionalized composites, the intensity of the peak at 1090 cm^{-1} is similar that of the peak at 1112 cm^{-1} (Fig. 3b). However, in the case of the composite with non-functionalized 3D-MoS₂ nanoflowers, the intensity of these peaks is different and also in the P3HT, which corroborates that the functionalization of 3D-MoS₂ nanoflowers increases their incorporation and interaction into P3HT. In the P3HT/MoS₂-EF and P3HT/MoS₂-CF composites, the vibration bands at 909 cm^{-1} and 656 cm^{-1} belonging to 3D-MoS₂ were more intense, especially in P3HT/MoS₂-EF, indicating a greater incorporation of 3D-MoS₂ into P3HT than for the P3HT/MoS₂-CF composite. The functionalized composites did not show bands belonging to the functionalizing agents. It has been reported that the bands in the characteristics of the carboxylic acid anchoring groups on TiO₂ belonging to P = O stretch and C = O stretch disappear when bonded to the metal oxide surface.⁶⁶

Based on the findings of Chen et al.,⁶⁷ the ratio between the intensities of the symmetric stretching C = C peak (1454 cm^{-1}) and the asymmetric stretching C = C peak (1510 cm^{-1}) can provide insights into the conjugation length of the polymer chain. A lower $I_{\text{sym}}/I_{\text{asym}}$ ratio indicates longer conjugation lengths and higher conductivity of the polymer chain. Table II presents the indicative conjugation lengths for P3HT and the functionalized and non-functionalized P3HT/MoS₂ composites. Both P3HT/MoS₂ and P3HT/MoS₂-CF (with a 2-thiophenecarboxylic acid functionalizing agent) exhibited the lowest conjugation length. Notably, the composite incorporating the functionalizing agent 2-hydroxy-2-(thiophene-3-yl)ethyl]phosphonate (P3HT/MoS₂-EF) demonstrated a conjugation length like that of P3HT.

In the P3HT/MoS₂-CF composite, the carboxyl group presented a planar configuration⁶⁸ and this probably formed a difficult conformation and stacking disorder in the P3HT/MoS₂-CF composite, which is why the conjugation length in the functionalized P3HT/MoS₂-CF composite is the largest, as indicated in Table II. On the other hand, the phosphonate group has a tetrahedral configuration and the structural diversity observed in metal phosphonates is mostly due to the multiple coordination modes of the tetrahedral

Table II Dyad and triad percent for P3HT and P3HT-MoS₂ composites

| Sample | $I_{\text{sym}}/I_{\text{asym}}$ |
|---------------------------|----------------------------------|
| P3HT | 2.01 |
| P3HT/MoS ₂ | 2.14 |
| P3HT/MoS ₂ -EF | 2.05 |
| P3HT/MoS ₂ -CF | 2.13 |

[R-PO₃]⁻² phosphonate binding units and resulting metal coordination possibilities, which contribute to the structural diversity of metal organic phosphonates.^{68,69} These most likely contribute to improving the conjugation length in P3HT/MoS₂-EF, which is very similar to P3HT.

X-Ray Diffraction

Figure 5 shows the XRD patterns of the 3D-MoS₂. The diffraction peaks at $2\theta = 14.1^\circ$, 33.4° , 39.8° , and 58.9° are in good agreement with the [002], [100] [103], and [110] crystallographic planes, respectively, which could be indexed to the hexagonal phase (JCPDS Card No.-37-1492).^{8,49,70} The interplanar spacing of the 3D-MoS₂ samples was calculated using the Bragg equation.⁸ The intense peak at 14.1° suggests many layers arranged along the [002] plane, for which the interplanar spacing of 3D-MoS₂ was found to be 6.28 \AA , a value within the reported range.^{8,49,71} A high-magnification TEM image, as shown in Fig. 2a, confirms the formation of 3D-MoS₂. On the other hand, P3HT exhibited characteristic peaks at $2\theta = 5.8^\circ$ and 23.4° , along with smaller peaks at $2\theta = 10.6^\circ$ and 16° . These peaks can be attributed to the Miller indices (100), (120), (200), and (111), respectively, which agree with the crystal system of P3HT, which is orthorhombic, as indicated by the P3HT:00-054-2080 reference card.

All P3HT/MoS₂ composites showed the diffraction peaks of P3HT at $2\theta = 5.8^\circ$, 10.6° , 16° , and 23.4° . In addition, they showed small peaks corresponding to 3D-MoS₂ nanoflowers at $2\theta = 14.1^\circ$, 33.4° , and 39.8° , the presence of

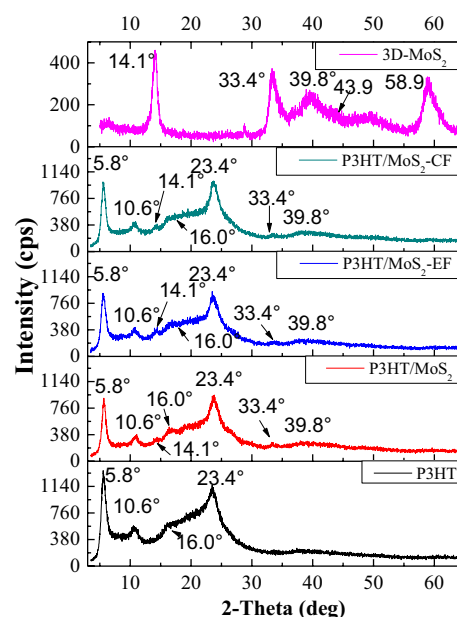


Fig. 5 XRD spectra of 3D-MoS₂, P3HT, and P3HT/MoS₂ composites with 3D-MoS₂ functionalized and non-functionalized.

these peaks corroborating the incorporation of 3D-MoS₂ in the polymer matrix. The presence of a crystalline phase in P3HT is confirmed by the peak reflection observed at 5.8° (α -axis orientation) and 23.4°. The orientation due to the 5.8° peak signifies that the main polymer chain is parallel to the substrate, while the side chains are perpendicular to it.⁷² When 3D-MoS₂ was added to P3HT, the intensity of the peak at 5.8° decreased a little, and the diffraction peak at $2\theta = 23.4^\circ$ was better defined, which indicates that the ordering of P3HT chains in the (120) plane is increased in the composites. It is worth mentioning that the P3HT/MoS₂-CF composite showed greater crystallinity than the P3HT/MoS₂ and P3HT/MoS₂-EF composites. The above behavior suggests that the incorporation of 3D-MoS₂ in P3HT modifies the ordering of the P3HT polymer chains. The P3HT/MoS₂-EF and P3HT/MoS₂-CF composites presented diffraction peaks at $2\theta = 14.1^\circ$, 33.4° , and 39.8° belonging to the 3D-MoS₂, and the functionalized composites presented diffraction peaks that were better defined than the composite with non-functionalized 3D-MoS₂. This suggests that functionalization of 3D-MoS₂ benefits the incorporation of 3D-MoS₂ in P3HT, which may be the carboxylic and phosphonic groups acting as either planar or tetrahedral coordination groups, resulting in different coordination possibilities for the phosphonic group; on the other hand, the carboxylic group may have less coordination possibilities due to planar configuration.

The crystal size was determined by the Scherrer equation, using as reference the diffraction plane at 5.8° corresponding to Miller index (100); the results are shown in Table III. The addition of unfunctionalized 3D-MoS₂ to P3HT leads to a decrease in crystal size from 9.69 nm for P3HT to 8.52 nm for the P3HT/MoS₂ composite. However, when functionalizing the 3D-MoS₂, an increase in crystal size was observed in the P3HT/MoS₂-EF and P3HT/MoS₂-CF composites. Therefore, the functionalization of the 3D-MoS₂ increases the crystal size of P3HT in the P3HT/MoS₂ composites.

UV-Visible Absorption

Figure 6 illustrates the UV-Vis spectra of 3D-MoS₂ in solution (inset), as well as films on glass substrates of P3HT and P3HT/MoS₂, P3HT/MoS₂-EF, and P3HT/MoS₂-CF

Table III Crystal size calculated by the Scherrer equation of P3HT and P3HT/MoS₂ composites

| Sample | Crystal size (nm) |
|---------------------------|-------------------|
| P3HT | 9.69 |
| P3HT/MoS ₂ | 8.52 |
| P3HT/MoS ₂ -EF | 9.79 |
| P3HT/MoS ₂ -CF | 10.25 |

composites. The spectra were measured in a wavelength range of 280–800 nm. In the case of P3HT, the π - π^* band exhibits a λ_{\max} at approximately 520 nm. When non-functionalized 3D-MoS₂ are incorporated into P3HT, the π - π^* band retains the same λ_{\max} . However, when functionalized 3D-MoS₂ are present, the composites spectra display a slight shift of the π - π^* band maximum to a higher wavelength (lower energy) at 525 nm. This shift suggests a reduced energy gap in the composites containing functionalized 3D-MoS₂. Furthermore, the presence of functionalized 3D-MoS₂ within P3HT leads to an increase in the absorption intensity of the π - π^* band, particularly noticeable in the P3HT/MoS₂-CF composite. This heightened absorption intensity can be attributed to the enhanced packing (compaction) of the P3HT polymer chains due to interactions between the functionalized 3D-MoS₂ and the P3HT chains. The composites containing functionalized 3D-MoS₂ exhibit more pronounced shoulder peaks at 550 nm and 602 nm in the π - π^* band (mostly P3HT/MoS₂-CF composite), indicative of a more favorable molecular arrangement compared to P3HT and P3HT/MoS₂.

It has been found that end functionalization of P3HT with carboxylic groups produces significantly hypsochromically shifted to the ultraviolet range in the maximum absorption peak when a carboxylic group is introduced to P3HT, which is due the carboxylic acids forming hydrogen bonds, fixing the polymer chain in a disordered conformation, and make stacking difficult, resulting in a decrease in the effective conjugation length.^{73–75} In our case, with in situ synthesis of the P3HT/MoS₂ composites under an inert atmosphere, the π - π^* stacking was maintained in the case of 3D-MoS₂ without functionalizing; however, when 3D-MoS₂ is functionalized, the stacking is improved, mainly in the P3HT/MoS₂-CF composite, which is related to the conjugation length in the

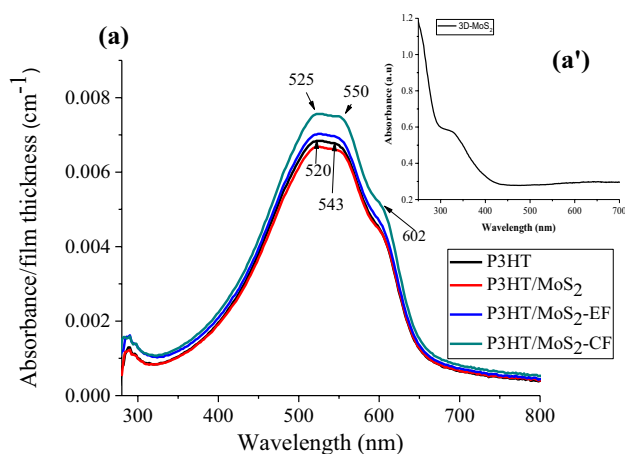


Fig. 6 (a) UV-Vis spectra of P3HT and non-functionalized and functionalized P3HT/MoS₂ composite films; a') inset 3D-MoS₂ in solution.

functionalized composites being enhanced compared to the non-functionalized composite, as indicated in Table II.

The UV–Vis spectra of the P3HT/MoS₂ composites do not show the absorption of 3D-MoS₂; a higher concentration is probably required to be appreciated.

The band gap energy (E_g) was calculated using Tauc plots. P3HT and P3HT/MoS₂ composites were considered as the semiconductor material of direct transition: $ODh\nu^2$ versus $h\nu$, where OD is the optical density and $h\nu$ is the photon energy.⁷⁶ The band gap values were 1.80 for 3D-MoS₂ in solution, in agreement with the literature for MoS₂ by the hydrothermal method.⁷⁷ Band gap values of 1.84 eV for P3HT and 1.84 eV, 1.82 eV, and 1.80 eV for P3HT/MoS₂, P3HT/MoS₂-EF and P3HT/MoS₂-CF composites in thin films, respectively, were determined. The presence of non-functionalized 3D-MoS₂ in P3HT did not cause any change in the band gap energy; however, when 3D-MoS₂ was functionalized it caused a decrease in the energy gap of P3HT, mostly in the P3HT/MoS₂-CF composite. The results of the energy band gap agreed with the XRD results, while the composites with functionalized 3D-MoS₂ presented a higher crystal size than the non-functionalized composites, which indicates a high ordering of polymer chains and therefore a large optical absorption at 602 nm.

Thermogravimetric Analysis

The thermal stability of 3D-MoS₂ is shown in Fig. 7. The 3D-MoS₂ showed a gradual weight loss of 4.65% from room temperature to 100°C, which can be attributed to the residual adsorbed water in the sample.^{78,79} The 3D-MoS₂ presented

two main weight losses with maximum decomposition temperature at 375°C and 602°C, similar behavior occurring for exfoliated nanosheets of MoS₂.⁸⁰ The first weight loss of 15.8 % at nearly 375°C is due to possible formation of molybdenum oxides and sulfur.^{78,79} The maximum weight loss of 26.75% at 600°C is associated with the 3D-MoS₂.

The thermal stability of P3HT and P3HT/MoS₂ composites is shown in Fig. 7. P3HT showed a unique weight loss with a maximum decomposition temperature of 487.93°C due to the P3HT decomposition, and showed thermal stability from room temperature to approximately 280.3°C. In the composites, the presence of 3D-MoS₂ caused a slight decrease in thermal stability, before the decomposition temperature of the P3HT chains, the graphs of composites showing thermal stability from room temperature to approximately 277.7°C. All *a'*) inset composites presented two main weight losses with maximum decomposition temperatures of 477.6°C and 640.4°C for the composite P3HT/MoS₂, 483.2°C and 679.7°C for the composite P3HT/MoS₂-CF, and 488.5°C and 647.5°C for the composite P3HT/MoS₂-EF. When the 3D-MoS₂ was not functionalized, the maximum decomposition temperature of P3HT in the P3HT/MoS₂ composite was lower (477.6°C) than the maximum decomposition temperature of P3HT (488.5°C). When functionalized 3D-MoS₂ was incorporated into the composites, the maximum decomposition temperature increased in comparison with the non-functionalized composites: P3HT/MoS₂-CF (483.2°C) and P3HT/MoS₂-EF (488.5°C), the latter being identical to that of P3HT. The P3HT/MoS₂ composites showed small weight losses before the weight loss of P3HT with maximum decomposition temperatures at: 387°C

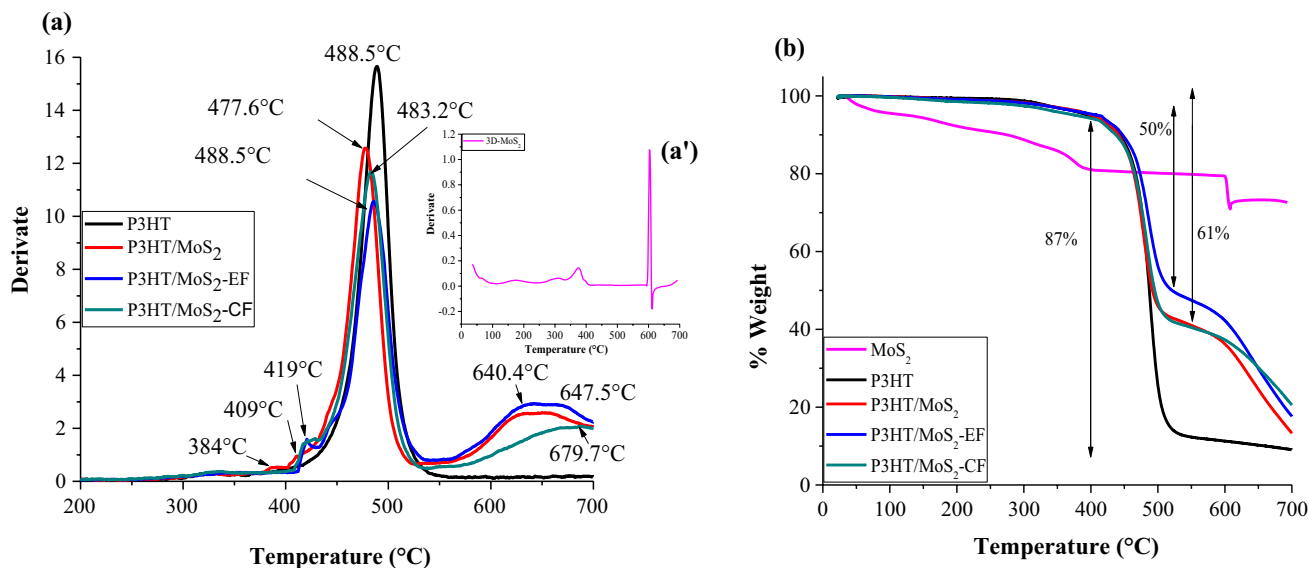


Fig. 7 (a) TGA curves of derivate vs. temperature of P3HT and P3HT/MoS₂ composites; *a'*) inset derivate vs. temperature 3D-MoS₂ (*a'*); and (b) % weight vs. temperature of P3HT and P3HT/MoS₂ composites.

and 409°C for P3HT/MoS₂, 420°C for P3HT/MoS₂-EF, and 429°C for P3HT/MoS₂-CF. This could be due to the weight loss of 375°C observed in 3D-MoS₂, which was displaced at the higher temperature in the composites, especially in the functionalized ones. Furthermore, the composites showed a third broad decomposition stage that began at approximately at 560°C due, on the one hand, to the presence of 3D-MoS₂ (decomposition temperature at 602°C), and, on the other hand, to the decomposition of the P3HT chains that interact with 3D-MoS₂, which decomposes at a higher temperature than P3HT chains without interacting with 3D-MoS₂. The decomposition maxima were observed at 640.4°C for P3HT/MoS₂, 647.5°C for P3HT/MoS₂-EF, and 679.7°C for P3HT/MoS₂-CF. An increase in this decomposition temperature was also observed in the composites compared to 3D-MoS₂, mostly in the P3HT/MoS₂-CF composite, which showed a greater interaction between the two materials. The broad signal of this decomposition temperature in the composites probably indicates that, in addition to the decomposition of 3D-MoS₂, there is decomposition at different temperatures of the chains that interacted with the 3D-MoS₂, those with a greater interaction decomposing at a higher temperature. The above corroborates the greater interaction of MoS₂ with the polymer chains in the P3HT/MoS₂-CF composites, which are those functionalized with 2-thiophenecarboxylic acid. Likewise, it is observed that the incorporation of MoS₂-CF in P3HT improves the thermal stability of the P3HT chains. As seen in Fig. 7b, the residual material of P3HT at 700°C was approximately 9.2%, that of the non-functionalized composite was 13.4%, and of the functionalized composites it was 18% (P3HT/MoS₂-EF) and 20.7% (P3HT/MoS₂-CF). It demonstrates a greater incorporation of MoS₂ in the functionalized composites, mostly in the P3HT/MoS₂-CF composite.

Cyclic Voltammetry

Figure 8 shows current–potential curves of spin-coated films of P3HT and P3HT/MoS₂ composites and 3D-MoS₂. The potential was scanned in the range of – 200 to 1200 mV at a scan rate of 20 mV/s.

The P3HT and P3HT/MoS₂ composite films showed electrochromic behavior, presenting color changes during potential scanning and oxidative doping and reductive de-doping of the conjugated system. Figure 8 shows a cyclic voltammogram of P3HT film, in which two oxidation peaks can be observed at 0.20 V and 0.75 in black and blue, respectively, and their respective reduction peaks in red and black at 0.10 V and 0.41 V, respectively, which are in agreement with Kim et al.⁸¹ New oxidation or reduction peaks were not detected in the cyclic voltammograms of the P3HT/MoS₂ composites. However, the presence of 3D-MoS₂ in P3HT generated a shift of the oxidation and

reduction peaks. The second oxidation peak shifted towards a higher potential in the functionalized composites, but in the unfunctionalized composite, it shifted towards a lower potential, indicating that the functionalization of 3D-MoS₂ causes its greater anchoring to the polymer chains, which is reflected in increasing the oxidation potential of the P3HT chains. Broadening and shifting of oxidation peaks were observed, especially in the functionalized composites, due to the greater anchoring of the 3D-MoS₂ with the P3HT chains.

The reduction peaks of the functionalized composites occurred at a lower voltage than in P3HT. All these changes are due to the interaction of the 3D-MoS₂ with the P3HT. Similar behavior has been observed.^{82–84}

When adding 3D-MoS₂, the composite P3HT/MoS₂ showed two oxidation peaks at lower voltage currents (0.17 V in black and 0.68 V in blue), and one reduction peak at 0.43 V. In the functionalized composites, especially in the P3HT/MoS₂-CF, two oxidation peaks can be observed at higher voltage currents (0.21 V in black and 0.85 V in blue), and, in the corresponding reduction peaks, a shift was observed at slightly lower voltage currents (0.04 V (red) and 0.31 V (black)). The addition of 3D-MoS₂ into P3HT clearly demonstrates alterations in the electronic configuration of P3HT, in agreement with Chaundhary et al.⁸³ The P3HT/MoS₂-EF composite presents the highest oxidation potential, and the closed range of oxidation potential confirms the closest interaction between P3HT and 3D-MoS₂. Normally, P3HT with high regioregularity contains a narrow range of conjugation lengths and is expected to have a closed range of oxidation potentials,⁸⁵ these results agreeing with the conjugation lengths and dyad percentages (%HT). Likewise, it is observed that the cycle area decreases with the addition of 3D-MoS₂ in P3HT, while the P3HT/MoS₂-CF composite presented a lower cycle area than P3HT, indicating an incorporation of charge, like P3HT in film. The above makes this material suitable for applications in electronics devices. The P3HT/MoS₂-CF presented the lowest cycle area probably due to a better interaction with 3D-MoS₂ nanoflowers (Table IV).

Figure 9 shows the electrical conductivity in darkness and illumination of P3HT and P3HT/MoS₂ composites. The electrical conductivity of P3HT increased with the incorporation of 3D-MoS₂. A higher conductivity in darkness and illumination was obtained in the P3HT/MoS₂ composites, with the composite P3HT/MoS₂-EF having the highest conductivity. This corroborates diethyl [2-hydroxy-2-(thiophene–3-yl)ethyl] phosphonate as a functionalization agent achieving a better dispersion of the 3D-MoS₂ within the polymer matrix, while a greater contact area between the P3HT and 3D-MoS₂ benefits the conductivity of the composite. This result agrees with what was obtained in conjugation length, %HT, and cyclic voltammetry. The photoresponses of P3HT/MoS₂-CF and P3HT/MoS₂ were like that of P3HT; however, it decreased

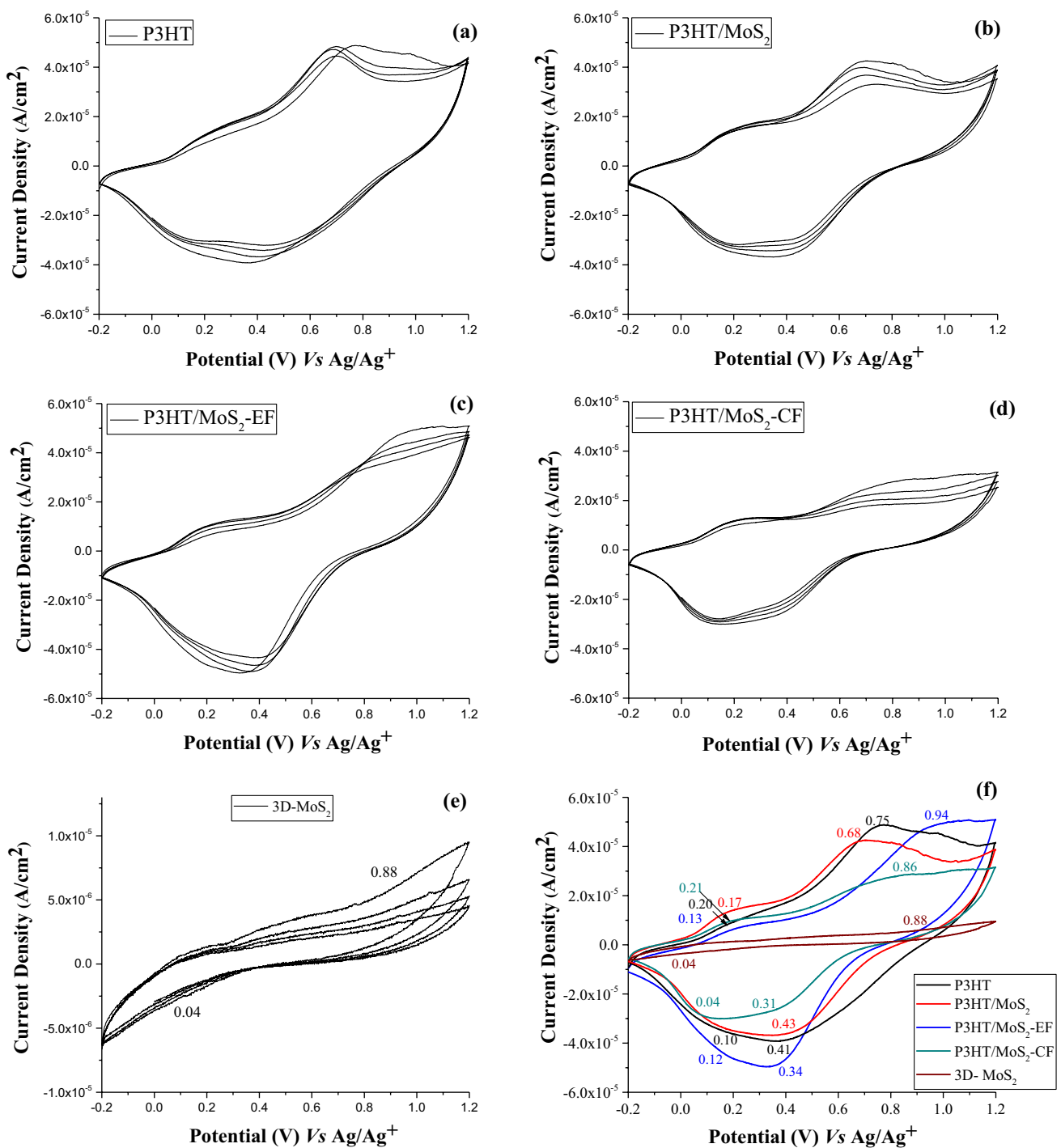


Fig. 8 Cyclic voltammogram of P3HT, non-functionalized, functionalized P3HT/MoS₂ composites, and 3D-MoS₂ for a potential range of – 200 to 1200 mV: (a–e) 4 cycles for each sample and (f) second cycle for each sample.

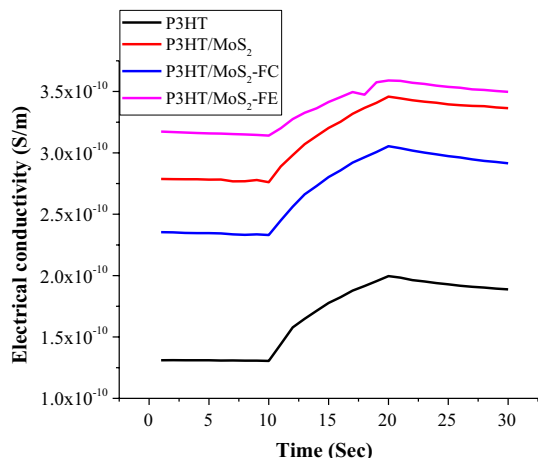
especially in the P3HT/MoS₂-EF composite, the latter presenting the lowest photoresponse (Table V). It has been reported that an increase of dark conductivity exhibits only weak photosensitivity,^{86,87} which suggests that, in the P3HT/MoS₂-EF composite, the density of photogenerated carriers is the smallest compared with the density of generated carriers of P3HT,

due to the enlarged impurity state density, probably due to the high content of 3D-MoS₂ nanoflowers in the composite.

The results reflect the potential of the new P3HT-MoS₂ composites for applications in optoelectronic devices. For example, in applications in electrochromic devices, the

Table IV Area of the first cycle of P3HT and P3HT/MoS₂ composites

| Sample | A _{TOT} (mA × mV/ cm ²) |
|---------------------------|--|
| P3HT | 0.06706 |
| P3HT/MoS ₂ | 0.06081 |
| P3HT/MoS ₂ -CF | 0.04595 |
| P3HT/MoS ₂ -EF | 0.06226 |

**Fig. 9** Electrical conductivity of P3HT and P3HT-MoS₂ composites in the dark and illumination.**Table V** Maximum values of electrical conductivity and photoresponse of P3HT and P3HT-MoS₂ composites

| SAMPLE | σ_{OFF} (S/m) | σ_{ON} (S/m) | Photoresponse |
|---------------------------|-----------------------------|----------------------------|-----------------------|
| P3HT | 1.30×10^{-10} | 2.00×10^{-10} | 7.0×10^{-11} |
| P3HT/MoS ₂ | 2.78×10^{-10} | 3.46×10^{-10} | 6.8×10^{-11} |
| P3HT/MoS ₂ -CF | 2.35×10^{-10} | 3.05×10^{-10} | 7.0×10^{-11} |
| P3HT/MoS ₂ -EF | 3.16×10^{-10} | 3.60×10^{-10} | 4.4×10^{-11} |

incorporation of 3D-MoS₂ in P3HT is likely to benefit the stability of the device.

Conclusions

One-step hydrothermal synthesis was employed to synthesize 3D-MoS₂ with a diameter of approximately 1–3 μm . The nanoflowers were successfully functionalized using diethyl[2-hydroxy-2-(thiophen-3-yl)ethyl] phosphonate and 2-thiophene carboxylic acid. The polymerization of P3HT was achieved in the presence of 3D-MoS₂ through Grignard metathesis. Analysis using FTIR, UV-Vis, and TEM confirmed the presence of 3D-MoS₂ in the P3HT/MoS₂ composites. Functionalization of 3D-MoS₂

improved their dispersion within the P3HT polymer matrix. Likewise, the functionalization of 3D-MoS₂ in the P3HT/MoS₂ composites could improve the interaction between P3HT and the 3D-MoS₂, increase the crystal size, absorbance, and conductivity, and promote the preservation of regioregularity and conjugation length, especially in the P3HT/MoS₂-EF composite. Likewise, with the functionalization of 3D-MoS₂, it was possible to reduce the energy gap of P3HT in the composites. Our work provides evidence for a greater performance in composites functionalized with the phosphonate group because a phosphonic anchor provides strong electronic coupling with the 3D-MoS₂. These composites can be used in flexible electronics photosensors, photocatalysis, and for harvesting energy material in solar cells.

Acknowledgments S. García-Carvajal thanks DGAPA-UNAM and CONACYT for the postdoctoral scholarship provided. Thanks to PAPIIT-DGAPA: IN112921 and IN114124 for the financial support and to Lourdes Palma-Tirado for TEM measurements and Ma. Christian Albor-Cortés for X-Ray measurements.

Conflict of interest The authors declare that they have not conflict of interest.

Open Access This article is licensed under a Creative Commons Attribution 4.0 International License, which permits use, sharing, adaptation, distribution and reproduction in any medium or format, as long as you give appropriate credit to the original author(s) and the source, provide a link to the Creative Commons licence, and indicate if changes were made. The images or other third party material in this article are included in the article's Creative Commons licence, unless indicated otherwise in a credit line to the material. If material is not included in the article's Creative Commons licence and your intended use is not permitted by statutory regulation or exceeds the permitted use, you will need to obtain permission directly from the copyright holder. To view a copy of this licence, visit <http://creativecommons.org/licenses/by/4.0/>.

References

1. V.P. Kumar and D.K. Panda, Review next generation 2D material molybdenum disulfide (MoS₂): properties, applications and challenges. *ECS J. Solid State Sci. Technol.* 11, 033012 (2022).
2. D.J. Trainer, Y. Zhang, F. Bobba, X. Xi, S.W. Hla, and M. Iavarone, The effects of atomic-scale strain relaxation on the electronic properties of monolayer MoS₂. *ACS Nano* 13, 8284 (2019).
3. N. Mphuthi, L. Sikhwivhilu, and S.S. Ray, Functionalization of 2D MoS₂ nanosheets with various metal and metal oxide nanostructures: their properties and application in electrochemical sensors. *Biosensors* 12(6), 386 (2022).
4. H. Zhu, Z. Hong, C. Zhou, Q. Wu, T. Zheng, L. Yang, S. Lan, and W. Yang, Energy band alignment of 2D/3D MoS₂/4H-SiC heterostructure modulated by multiple interfacial interactions. *Front. Phys.* 18(1), 13301 (2023).
5. N. Alinejadian, L. Kollo, and I. Odnevall, Progress in additive manufacturing of MoS₂-based structures for energy storage applications—a review. *Mater. Sci. Semicond. Process.* 1(139), 106331 (2022).

6. C. Vidya, C. Manjunatha, A. Pranjal, I. Faraaz, and K. Prashantha, A multifunctional nanostructured molybdenum disulphide (MoS₂): an overview on synthesis, structural features, and potential applications. *Mater. Res. Innov.* 27, 177 (2023).
7. A. Joseph, K.K. Tadi, K.S. Anju, and P.M. Aneesh, Structural, optical, magnetic, and electrochemical properties of hydrothermally synthesized WS₂ nanoflakes. *J. Mater. Res.* 36(884–895), 884 (2021).
8. M. Baby and K. Rajeev Kumar, Structural and optical characterization of stacked MoS₂ nanosheets by hydrothermal method. *J. Mater. Sci. Mater. Electron.* 29, 4658 (2018).
9. B. Yulianto, N.L.W. Septiani, Y.V. Kaneti, M. Iqbal, G. Gumilar, M. Kim, J. Na, K.C.W. Wu, and Y. Yamauchi, Green synthesis of metal oxide nanostructures using naturally occurring compounds for energy, environmental, and bio-related applications. *NJC.* 43, 15846 (2019).
10. S. Anwer, Y. Huang, B. Li, B. Govindan, K. Liao, J.W. Cantwell, F. Wu, R. Chen, and L. Zheng, Nature-inspired, graphene-wrapped 3D MoS₂ ultrathin microflower architecture as a high-performance anode material for sodium-ion batteries. *ACS Appl. Mater. Interfaces* 11(25), 22323 (2019).
11. Y. Chao, Y. Ge, Z. Chen, X. Cui, C. Zhao, C. Wang, and G.G. Wallace, One-pot hydrothermal synthesis of solution-processable MoS₂/PEDOT:PSS composites for high-performance supercapacitors. *ACS Appl. Mater. Interfaces* 13, 7285 (2021).
12. Y. Cheng, K. Pang, X. Wu, Z. Zhang, X. Xu, J. Ren, W. Huang, and R. Song, In situ hydrothermal synthesis MoS₂/guar gum carbon nanoflowers as advanced electrocatalysts for electrocatalytic hydrogen evolution. *ACS Sustain. Chem. Eng.* 6, 8688 (2018).
13. E. Singh, K.S. Kim, G.Y. Yeom, and H.S. Nalwa, Atomically thin-layered molybdenum disulfide (MoS₂) for bulk-heterojunction solar cells. *ACS Appl. Mater. Interfaces* 9, 3223 (2017).
14. J. Singh, S. Kumar, and R.K. Soni, Synthesis of 3D-MoS₂ nanoflowers with tunable surface area for the application in photocatalysis and SERS based sensing. *J. Alloys Compnd.* 30(849), 156502 (2020).
15. Y. Zhang, W. Zeng, and Y. Li, The hydrothermal synthesis of 3D hierarchical porous MoS₂ microspheres assembled by nanosheets with excellent gas sensing properties. *J. Alloys Compd.* 749, 355 (2018).
16. X. Feng, X. Wang, W. Xing, K. Zhou, L. Song, and Y. Hu, Liquid-exfoliated MoS₂ by chitosan and enhanced mechanical and thermal properties of chitosan/MoS₂ composites. *Compos. Sci. Technol.* 93, 76 (2014).
17. M. Zhi, Q. Liu, Y. Zhao, S. Gao, Z. Zhang, and Y. He, Novel MoS₂-DOPO hybrid for effective enhancements on flame retardancy and smoke suppression of flexible polyurethane foams. *ACS Omega* 5, 2734 (2020).
18. K. Malkappa, S.S. Ray, and N. Kumar, Enhanced thermo-mechanical stiffness, thermal stability, and fire retardant performance of surface-modified 2D MoS₂ nanosheet-reinforced polyurethane composites. *Macromol. Mater. Eng.* 304(1), 1800562 (2019).
19. H. Peng, D. Wang, L. Zhang, M. Li, M. Liu, C. Wang, and S. Fu, Amorphous cobalt borate nanosheets grown on MoS₂ nanosheet for simultaneously improving the flame retardancy and mechanical properties of polyacrylonitrile composite fiber. *Compos. Part B Eng.* 15(201), 108298 (2020).
20. H. Peng, D. Wang, M. Li, L. Zhang, M. Liu, and S. Fu, N-P-Zn-containing 2D supermolecular networks grown on MoS₂ nanosheets for mechanical and flame-retardant reinforcements of polyacrylonitrile fiber. *J. Chem. Eng.* 372, 873 (2019).
21. L. He, F. Chu, X. Zhou, L. Song, and Y. Hu, Cactus-like structure of BP@ MoS₂ hybrids: An effective mechanical reinforcement and flame retardant additive for waterborne polyurethane. *Polym. Degrad. Stab.* 1(202), 110027 (2022).
22. A. Abun, B.R. Huang, A. Saravanan, D. Kathiravan, and P.D. Hong, Effect of PMMA on the surface of exfoliated MoS₂ nanosheets and their highly enhanced ammonia gas sensing properties at room temperature. *J. Alloys Compnd.* 15(832), 155005 (2020).
23. A. Liu, S. Lv, L. Jiang, F. Liu, L. Zhao, J. Wang, X. Hu, Z. Yang, J. He, C. Wang, and X. Yan, The gas sensor utilizing polyaniline/MoS₂ nanosheets/SnO₂ nanotubes for the room temperature detection of ammonia. *Sens. Actuators B Chem.* 1(332), 129444 (2021).
24. N. Goel, J. Bera, R. Kumar, S. Sahu, and M. Kumar, MoS₂-PVP nanocomposites decorated ZnO microspheres for efficient hydrogen detection. *IEEE Sens. J.* 21, 8878 (2021).
25. M.S. Ahmad, M.M. Shahid, S. Shahabuddin, K. Munawar, N.A. Rahim, and W. Ahmed, Effect of concentration of MoS₂ on the TCO-Pt free polyaniline nano-rod based counter electrode for dye sensitized solar cell application. *Mater. Technol.* 37, 1366 (2022).
26. U. Ghafoor, A.B. Aqeel, U.K. Zaman, T. Zahid, M. Noman, and M.S. Ahmad, Effect of molybdenum disulfide on the performance of polyaniline based counter electrode for dye-sensitized solar cell applications. *Energies* 14(13), 3786 (2021).
27. A. Asok, A.A. Naik, S. Arunachalam, R. Govindaraj, and K. Haribabu, Microwave assisted synthesis of polythiophene-molybdenum sulfide counter electrode in dye sensitized solar cell. *J. Mater. Sci. Mater. Electron.* 30(30), 13655 (2019).
28. S. Chatterjee, S. Jinnai, and Y. Ie, Nonfullerene acceptors for P3HT-based organic solar cells. *J. Mater. Chem. A Mater.* 9, 18857 (2021).
29. R. Ray, A.S. Sarkar, and S.K. Pal, Improving carrier transport in polymer films by incorporating MoS₂ nanosheets. *J. Phys. D Appl. Phys.* 53(27), 275109 (2020).
30. A. Verma, P.K. Sahu, V. Chaudhary, A.K. Singh, V.N. Mishra, and R. Prakash, Fabrication and characterization of P3HT/MoS thin-film based ammonia sensor operated at room temperature. *IEEE Sens. J.* 22, 10361 (2022).
31. T. Xie, G. Xie, Y. Su, D. Hongfei, Z. Ye, and Y. Jiang, Ammonia gas sensors based on poly (3-hexylthiophene)-molybdenum disulfide film transistors. *Nanotechnology* 27, 065502 (2016).
32. S. Kandpal, T. Ghosh, C. Rani, S. Rani, D.K. Pathak, M. Tanwar, R. Bhatia, I. Sameera, and R. Kumar, MoS₂ nano-flower incorporation for improving organic-organic solid state electrochromic device performance. *Solar Energy Mater. Solar Cells.* 1(236), 111502 (2022).
33. S. Kandpal, T. Ghosh, C. Rani, S. Rani, L. Bansal, M. Tanwar, R. Bhatia, I. Sameera, and R. Kumar, MoS₂ doping and concentration optimization for application-specific design of P3HT-viologen-based solid state electrochromic device. *J. Phys. D Appl. Phys.* 55(37), 375101 (2022).
34. S.P. Tiwari, R. Verma, M.B. Alam, R. Kumari, O.P. Sinha, and R. Srivastava, Charge transport study of P3HT blended MoS₂. *Vacuum* 146, 474 (2017).
35. N. Kim, Molybdenum Disulphide (MoS₂)-Poly(3-hexylthiophene) (P3HT) Hybrid Ink for Printed Thin-Film Transistor *Appl.* (2020).
36. V. Chaudhary, R.K. Pandey, R. Prakash, N. Kumar, and A.K. Singh, Unfolding photophysical properties of poly (3-hexylthiophene)-MoS₂ organic-inorganic hybrid materials: an application to self-powered photodetectors. *Nanotechnology* 32(38), 385201 (2021).
37. F.N. Sari, Y.C. Liu, and J.M. Ting, Synthesis of MoS₂/MoO₃ or P3HT nanocomposites consisting of sandwich-like structures via environmental benign supercritical fluid CO₂ and its use in supercapacitor. *Compos. Part B Eng.* 15(177), 107355 (2019).
38. R. Ray, A.S. Sarkar, and S.K. Pal, Improving performance and moisture stability of perovskite solar cells through interface engineering with polymer-2D MoS₂ nanohybrid. *J. Sol. Energy* 193, 95 (2019).

39. S. Kandpal, T. Ghosh, C. Rani, M. Tanwar, M. Sharma, S. Rani, D.K. Pathak, R. Bhatia, I. Sameera, J. Jayabalan, and R. Kumar, Bifunctional application of viologen-MoS₂-CNT/polythiophene device as electrochromic diode and half-wave rectifier. *ACS Mater. Au.* 2(3), 293 (2022).
40. B. Sun, Z. Su, Y. Hao, J. Pei, and Y. Li, Facile fabrication of MoS₂-P3HT hybrid microheterostructure with enhanced photovoltaic performance in TiO₂ nanorod array based hybrid solar cell. *Solid State Sci.* 94, 92 (2019).
41. K. Zhou, J. Liu, P. Wen, Y. Hu, and Z. Gui, A noncovalent functionalization approach to improve the dispersibility and properties of polymer/MoS₂ composites. *Appl. Surf. Sci.* 316, 237 (2014).
42. X. Wang, W. Xing, X. Feng, L. Song, and Y. Hu, MoS₂/polymer nanocomposites: preparation, properties, and applications. *Polym. Eng. Rev.* 57, 440 (2017).
43. A. Sethulekshmi, J. Jayan, S. Appukuttan, and J. Kuruvilla, MoS₂: Advanced nanofiller for reinforcing polymer matrix. *Phys. E Low-Dimens. Syst. Nanostruct.* 132, 114716 (2021).
44. S. García-Carvajal, M.E. Nicho, I. Linzaga-Elizalde, D. Romero-Borja, J.L. Maldonado, F. Hernández-Guzmán, M. Fuentes-Pérez, and D. Hernández-Martínez, Effect of processing parameters on polymerization of P3HT in presence of CdS. *J. Electron. Mater.* 48, 8212 (2019).
45. S. García-Carvajal, D. Hernández-Martínez, I. Linzaga-Elizalde, J.L. Maldonado, P. Altuzar-Coello, and M.E. Nicho, Effect of the functionalization of CdS nanoparticles in the in situ synthesis of P3HT/CdS composites. *Eur. Polym. J.* 116, 471 (2019).
46. H. Ma, H. Gao, Z. Zhou, W. Xu, and F. Ren, Direct synthesis of P3HT/CdS nanocomposites with end-functionalized P3HT as the template. *Polym. Polym. Compos.* 23(7), 435 (2015).
47. F. Monnaie, W. Brullot, T. Verbiest, J. de Winter, P. Gerbaux, A. Smeets, and G. Koeckelberghs, Synthesis of end-group functionalized P3HT: General protocol for P3HT/nanoparticle hybrids. *Macromolecules* 46, 8500 (2013).
48. E.B. Pentzer, F.A. Bokel, R.C. Hayward, and T. Emrick, Nanocomposite “superhighways” by solution assembly of semiconductor nanostructures with ligand-functionalized conjugated polymers. *Adv. Mater.* 24, 2254 (2012).
49. J.H. Huang, M.A. Ibrahim, and C.W. Chu, Interfacial engineering affects the photocatalytic activity of poly(3-hexylthiophene)-modified TiO₂. *RSC Adv.* 3, 26438 (2013).
50. X. Zhang, X. Huang, M. Xue, X. Ye, W. Lei, H. Tang, and C. Li, Hydrothermal synthesis and characterization of 3D flower-like MoS₂ microspheres. *Mater. Lett.* 148, 67 (2015).
51. I. Linzaga-Elizalde, J. Escalante, M.E. Nicho, and M. Güizado-Rodríguez, Synthesis of 2-(Thiophen-3-yl)vinylphosphonic acid. *Synth. Commun.* 39, 1511 (2009).
52. F. Hernández-Guzmán, M.E. Nicho-Díaz, A. Medrano-Solís, and P. Altuzar-Coello, In situ synthesis by Grignard Metathesis of poly(3-hexylthiophene) in presence of CdS and their properties. *Eur. Polym. J.* 90, 407 (2017).
53. R. Senthilkumar, S. Ramakrishnan, M. Balu, P.C. Ramamurthy, D. Kumaresan, and N.K. Kothurkar, One-step hydrothermal synthesis of marigold flower-like nanostructured MoS₂ as a counter electrode for dye-sensitized solar cells. *J. Solid State Electrochem.* 22, 3331 (2018).
54. D. Presto, V. Song, and D. Boucher, P3HT/graphene composites synthesized using In situ GRIM methods. *J. Polym. Sci. B Polym. Phys.* 55, 60 (2017).
55. H. Zhang, H. Zhang, X. Zhang, T. Sun, M. Liang, Y. Chen, Z. Heng, and H. Zou, In situ self-assembled block copolymer nanowires on high-modulus carbon fibers surface for enhanced interfacial performance of CFRPs. *Chem. Eng. J.* 1(451), 138583 (2023).
56. V. Saini, Z. Li, S. Bourdo, E. Dervishi, Y. Xu, X. Ma, V.P. Kunets, G.J. Salamo, T. Viswanathan, A.R. Biris, D. Saini, and A.S. Biris, Electrical, optical, and morphological properties of p3ht-mwnt nanocomposites prepared by In situ polymerization. *J. Phys. Chem. C* 113, 8023 (2009).
57. H.P. Barrett, W.J. Kennedy, and D.S. Boucher, Spectroscopic characterization of P3HT/SWNT composites synthesized using in situ GRIM methods: Improved polymer ordering via nanoscaffolding. *J Polym Sci B* 52, 310 (2014).
58. H.T.T. Duong, Y. Chen, S.A. Tawfik, S. Wen, M. Parviz, O. Shimoni, and D.J. Ab, Systematic investigation of functional ligands for colloidal stable up conversion nanoparticles. *RSC Adv.* 8(4842–4849), 4842 (2018).
59. L. Zhang and J.M. Cole, Anchoring groups for dye-sensitized solar cells. *ACS Appl. Mater. Interfaces* 7, 3427 (2015).
60. Y.K. Han, Y.J. Lee, and P.C. Huang, Regioregularity effects in poly(3-hexylthiophene): PCBM-based solar cells incorporating acid-doped polyaniline nanotubes as an interfacial layer. *J. Electrochem. Soc.* 156(4), K37 (2009).
61. H. Huang, C. Du, H. Shi, X. Feng, J. Li, Y. Tan, and W. Song, Water-soluble monolayer molybdenum disulfide quantum dots with up conversion fluorescence. *Part. Part. Syst. Charact.* 32, 72 (2015).
62. E.M. Mkawi, Y. Al-Hadeethi, R.S. Bazuhair, A.S. Yousef, E. Shalaan, B. Arkook, A.M. Abdeldaiem, R. Almalki, and E. Bekyarova, Optimization of Sb₂S₃ nanocrystal concentrations in P3HT: PCBM layers to improve the performance of polymer solar cells. *Polymers* 13(13), 2152 (2021).
63. B. Yedikardeş, F. Ordokhani, N. Akkan, E. Kurt, N.K. Yavuz, E. Zayim, and M. Altun, Enhanced electrical properties of P3HT:WO₃ hybrid thin film transistors. *J. Electron. Mater.* 50, 2466 (2021).
64. E.M. Mkawi, Y. Al-Hadeethi, R.S. Bazuhair, E. Shalaan, B. Arkook, A.M. Abdel-Daiem, and E. Bekyarova, Fabricated Cu₂Zn SnS₄ (CZTS) nanoparticles as an additive in P3HT: PCBM active layer for efficiency improvement of polymer solar cell. *J. Lumin.* 1(240), 118420 (2021).
65. W. Jaimes, G. Alvarado-Tenorio, C. Martínez-Alonso, A. Quevedo-López, H. Hu, and M.E. Nicho, Effect of CdS nanoparticle content on the in situ polymerization of 3-hexylthiophene-2,5-diyl and the application of P3HT-CdS products in hybrid solar cells. *Mater. Sci. Semicond. Process.* 37, 259 (2015).
66. K.L. Materna, R.H. Crabtree, and G.W. Brudvig, Anchoring groups for photocatalytic water oxidation on metal oxide surfaces. *Chem. Soc. Rev.* 46, 6099 (2017).
67. T.A. Chen, X. Wu, and R.D. Rieke, Regiocontrolled synthesis of poly(3-alkylthiophenes) mediated by Rieke zinc: their characterization and solid-state properties. *J. Am. Chem. Soc.* 117(1), 233 (1995).
68. G. Yücesan, Y. Zorlu, M. Stricker, and J. Beckmann, Metal-organic solids derived from arylphosphonic acids. *Coord. Chem. Rev.* 369, 105 (2018).
69. J.L. Viveros-Ceballos, C. Cativiela, and M. Ordóñez, One-pot three-component highly diastereoselective synthesis of isoindolin-1-one-3-phosphonates under solvent and catalyst free-conditions. *Tetrahedron Asymmetry* 22, 1479 (2011).
70. H. Lin, X. Chen, H. Li, M. Yang, and Y. Qi, Hydrothermal synthesis, and characterization of MoS₂ nanorods. *Mater. Lett.* 64, 1748 (2010).
71. R. Senthilkumar, M. Balu, S. Ramakrishnan, P.C. Ramamurthy, S.K. Batabyal, D. Kumaresan, and N.K. Kothurkar, Molybdenum disulfide/reduced graphene oxide hybrids with enhanced electrocatalytic activity: an efficient counter electrode for dye-sensitized solar cells. *J. Electroanal. Chem.* 15(847), 113236 (2019).
72. M. Fuentes-Pérez, M.E. Nicho, M. Sotelo-Lerma, J.L. Fuentes-Ríos, J. Castellón-Urbe, U. León-Silva, F. Hernández-Guzmán, and S. García-Carvajal, Influence of the FeO(OH) nanoparticles

- concentration in the in situ synthesis of P3HT. *Eur. Polym. J.* 99, 172 (2018).
73. J. Zhang, H. Yang, S. Xu, L. Yang, Y. Song, L. Jiang, and Y. Dan, Dramatic enhancement of visible light photocatalysis due to strong interaction between TiO₂ and end-group functionalized P3HT. *Appl. Catal. B* 174, 193 (2015).
 74. R.H. Lohwasser, J. Bandara, and M. Thelakkat, Tailor-made synthesis of poly(3-hexylthiophene) with carboxylic end groups and its application as a polymer sensitizer in solid-state dye-sensitized solar cells. *J. Mater. Chem.* 19, 4126 (2009).
 75. B.A. Priya, T. Sivakumar, and P. Venkateswari, Construction of MoS₂ nanoparticles incorporated TiO₂ nanosheets heterojunction photocatalyst for enhanced visible light driven hydrogen production. *Inorg. Chem. Commun.* 1(136), 109118 (2022).
 76. J. Tauc, R. Grigorovici, and A. Vancu, TAUC: optical properties and electronic structure of Ge optical properties and electronic structure of amorphous germanium. *Phys. Stat. Sol.* 15(2), 627 (1966).
 77. N. Kumar, P. Siroha, H. Shankar, D. Singh, Y. Sharma, R. Kumar, N. Yadav, K.K. Dey, H. Borkar, and J. Gangwar, probing into crystallography and morphology properties of MoS₂ nanoflowers synthesized via temperature dependent hydrothermal method. *Nano Express.* 3(3), 035001 (2022).
 78. S. Mishra, P.K. Maurya, and A.K. Mishra, 2H-MoS₂ nanoflowers based high energy density solid state supercapacitor. *Mater. Chem. Phys.* 15(255), 123551 (2020).
 79. W. Peng, W. Wang, G. Han, Y. Huang, and Y. Zhang, Fabrication of 3D flower-like MoS₂/graphene composite as high-performance electrode for capacitive deionization. *Desalination* 1(473), 114191 (2020).
 80. K. Zhou, J. Liu, W. Zeng, Y. Hu, and Z. Gui, In situ synthesis, morphology, and fundamental properties of polymer/MoS₂ nanocomposites. *Compos. Sci. Technol.* 107, 120 (2015).
 81. T.H. Kim, S.H. Song, H.J. Kim, S.H. Oh, S.Y. Han, G. Kim, and Y.C. Nah, Effects of oxidation potential and retention time on electrochromic stability of poly (3-hexyl thiophene) films. *Appl. Surf. Sci.* 1(442), 78 (2018).
 82. A. Baray-Calderón, J. Camacho-Cáceres, F. Hernández-Guzmán, H. Hu, and M.E. Nicho, Enhanced performance of poly (3-hexylthiophene)-based electrochromic devices by adding a mesoporous TiO₂ layer. *Synth. Met.* 1(293), 117274 (2023).
 83. V. Chaudhary, R.K. Pandey, P.K. Sahu, R. Prakash, N. Kumar, and S.A. Kumar, MoS₂ assisted self-assembled poly (3-hexylthiophene) thin films at an air/liquid interface for high-performance field-effect transistors under ambient conditions. *J. Phys. Chem. C* 124(15), 8101 (2020).
 84. A. Gómez-Cortez, D. Hernández-Martínez, A. Baray-Calderón, P. Altuzar-Coello, M.C. Resendiz-González, and M.E. Nicho, Synthesis and characterization of novel P3HT-CuO composites for their application in electrochromic devices. *Synth. Met.* 1(300), 117487 (2023).
 85. F. Vergara-Juárez, A. Baray-Calderón, U. León-Silva, F. Delgado-Arroyo, and M.E. Nicho, Effect of incorporating silica extracted from natural source in poly (3-hexylthiophene-2, 5-diyl). *J. Polym. Res.* 28(12), 485 (2021).
 86. A. Baray-Calderón, P. Acevedo-Peña, O.A. Castelo-González, C. Martínez-Alonso, M. Sotelo-Lerma, M.C. Arenas-Arrocena, and H. Hu, Cationic and anionic modification of CdS thin films by surface chemical treatment. *Appl. Surf. Sci.* 475, 676 (2019).
 87. M.T.S. Nair, P.K. Nair, R.A. Zingaro, and E.A. Meyers, Conversion of chemically deposited photosensitive CdS thin films to n-type by air annealing and ion exchange reaction. *J. Appl. Phys.* 75, 1557 (1994).

Publisher's Note Springer Nature remains neutral with regard to jurisdictional claims in published maps and institutional affiliations.

Authors and Affiliations

S. García-Carvajal¹  · M. E. Nicho² · D. Hernández-Martínez³ · M. Fuentes-Pérez² · J. Nicasio-Collazo⁴ · V. Ruiz-Santoyo¹ · M. C. Arenas-Arrocena¹

✉ S. García-Carvajal
scarvajalg@enes.unam.mx

✉ M. C. Arenas-Arrocena
carenas@enes.unam.mx

¹ Escuela Nacional de Estudios Superiores Unidad León, Universidad Nacional Autónoma de México, Boulevard UNAM #2011 Col. Predio El Saucillo y El Potrero Comunidad de Los Tepetates, C. P. 37684 León, Guanajuato, México

² Centro de Investigación en Ingeniería y Ciencias Aplicadas, Universidad Autónoma del Estado de

Morelos, Av. Universidad 1001, Col. Chamilpa, C.P. 62209 Cuernavaca, Morelos, México

³ Departamento de Investigación en Polímeros y Materiales, Universidad de Sonora, Rosales y Blvd. Luis Encinas, C.P. 83000 Hermosillo, Sonora, México

⁴ Facultad de Estudios Superiores Cuautitlán, Universidad Nacional Autónoma de México, Av. 1° de Mayo S/N, Santa María las Torres, Campo Uno, C.P. 54740 Cuautitlán Izcalli, Estado de México, México